nature portfolio

https://doi.org/10.1038/s41561-021-00706-3

## Supplementary information

# A pole-to-equator ocean overturning circulation on Enceladus

In the format provided by the authors and unedited

**Supplemental Material**

# A pole-to-equator ocean overturning circulation on Enceladus

Ana H. Lobo*[1], Andrew F. Thompson[1], Steven D. Vance[2], and Saikiran Tharimena[2]

[1] *California Institute of Technology, Pasadena, CA, USA*
[2] *Jet Propulsion Laboratory, California Institute of Technology, Pasadena, CA 91109, USA*

Contact information:
Ana H. Lobo
California Institute of Technology
1200 E. California Blvd., M.C. 150-21
Pasadena, CA 91125
Email: lobo@caltech.edu

## S.1 Expanded Methods

In this section, we describe the governing equations of the spherical, zonally averaged, idealized overturning model. We begin with buoyancy conservation. Buoyancy is linearly related to density $\rho$ through the relationship,

$$b = g\left(\frac{\rho_0 - \rho}{\rho_0}\right), \tag{s1}$$

where $\rho_0$ is a reference density. The use of buoyancy emphasizes that differences in density constrain the overturning circulation as opposed to the absolute density.

Conservation of buoyancy is given by:

$$\frac{Db}{Dt} = -\nabla \cdot \mathbf{F_b} \approx -\frac{\partial F_b}{\partial z}, \tag{s2}$$

where $\mathbf{F_b}$ is the buoyancy flux. We apply the assumptions that the buoyancy flux at the ocean-ice interface decays to zero over the depth of the mixed layer, such that water mass transformation due to ocean-ice interactions is confined to this layer, and the vertical divergence of the vertical flux dominates $\nabla \cdot \mathbf{F_b}$ (right-hand side of eq. s2). The buoyancy flux varies with latitude and our sign convention is that $F_b(z=0) > 0$ produces more buoyant (lighter) water and $F_b(z=0) < 0$ produces less buoyant (denser) water. Expanding the material derivative, and applying a parameterization for the turbulent buoyancy flux in the ocean interior (discussed below), gives:

$$\begin{aligned}\frac{\partial b}{\partial t} &= -\mathbf{u}\cdot\nabla b - \nabla\cdot\mathbf{F_b} \qquad (s3)\\ &\approx \underbrace{-v\frac{\partial b}{\partial y} - w\frac{\partial b}{\partial z}}_{\text{advection}} + \underbrace{\frac{\partial}{\partial z}\left(\kappa\frac{\partial b}{\partial z}\right)}_{\text{interior mixing}} - \underbrace{\frac{\partial F_b}{\partial z}}_{\substack{\text{buoyancy}\\ \text{flux at}\\ \text{surface}}}.\end{aligned}$$

In steady state, $\partial b/\partial t = 0$ such that both adiabatic advection and diabatic mixing in the ocean interior are balanced by transformation at the ocean-ice interface. In other words, volume is conserved in each layer at steady state. The flow, represented by $v$ and $w$, is the total ocean circulation comprising both mean and eddy components, for example $v = \overline{v} + v'$. The total flow is more commonly referred to as the residual circulation in the oceanographic literature on water mass transformation due to the tendency for mean and eddy components to cancel in certain regions of the terrestrial ocean [1].

Assuming the upper part of Enceladus' ocean is zonally unbounded, the mean meridional velocity is weak and the meridional transport is dominated by eddy fluxes, e.g. $\overline{v'b'}$ and $\overline{w'b'}$. The mean meridional velocity, $\overline{v}$, vanishes in the absence of frictional forces because, assuming a small Rossby number, there is no zonally-averaged zonal pressure gradient to support this flow.

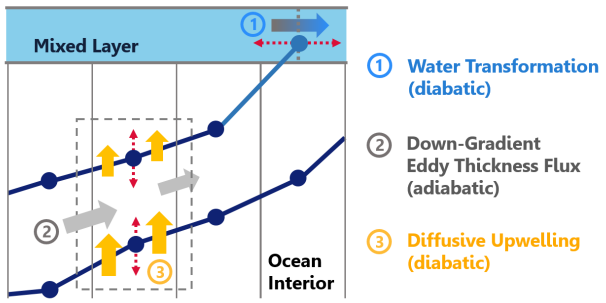


Fig. s1: Diagram of how physical processes are represented within the model grid. The dark blue dots indicate the depth of each layer that evolves with time. The position where the interface outcrops at the ocean-ice boundary (light blue dot) also evolves in time, independent of the grid. This figure is not drawn to scale.

We parameterize the eddy transport using a well-tested closure from the oceanographic literature [2], in which the adiabatic component of the advection arises from the relationship

$$\Psi_{\text{adiabatic}} = K_e s L, \tag{s4}$$

such that $v = -\partial\Psi/\partial z$ and $w = \partial\Psi/\partial y$. Here $s(y)$ is the slope of the interface separating density layers, $L(y)$ is the zonal length of each latitude circle, $\Psi$ is a streamfunction quantifying a volume transport, and $K_e$ is an isopycnal eddy diffusivity ($\mathrm{m^2\ s^{-1}}$). The eddy advection is assumed to act along density surfaces so that $v$ and $w$ combine to be parallel to the layer interfaces. Because the resulting flow is occurring within density layers, not involving mixing between different water classes, it is adiabatic in nature. In our model results, this flow can be thought of as a lateral flow, though it is technically parallel to isopycnals and not necessarily parallel to lines of constant depth. Note that while the slope of the density layers determines the intensity of the mesoscale eddies, the eddies act to transport tracers down large-scale gradients, such that a net volume transport is only possible when a layer-thickness gradient is present. If density layers are parallel (constant layer thickness), there remains an active eddy field, but there is no net volume transport. We set $K_e$ to an Earth-like value

(1000 $\mathrm{m^2\ s^{-1}}$) for the control simulation, and we test the sensitivity of the circulation to changes in $K_\mathrm{e}$.

An important assumption in these simulations is that $K_\mathrm{e}$ is uniform throughout the ocean. Mixing length theory is often employed to argue that the eddy diffusivity, which is caused predominantly by mesoscale eddies, scales as $K_\mathrm{e} \sim U\ell$, which depends on both the strength of the eddy velocities $U$ and the size of the eddy $\ell$ [3]. We can approximate the eddy mixing length as the Rossby deformation radius $R = NH\pi^{-1}f^{-1}$. Here, $f$ is the Coriolis parameter ($f = 2\Omega \sin\phi$) and $N^2 = \partial b/\partial z$. If we use $N^2 \approx \Delta B/H$ , where $H$ is the total ocean depth (30 km) and $\Delta B$ is the buoyancy difference between the lightest and densest layers, we would have $R = 10$ km in the midlatitudes. If we instead calculate $N$ based on our model output and use our deepest layer as a measure of the pycnocline, such that we can set $H$ to that layer's depth, this results in $R = 3$ km (at 45° latitude). Given that the total distance between the equator and pole on Enceladus is 395 km, this deformation radius provides reasonable support for a scale separation between the eddy and domain sizes and therefore justification for using an eddy diffusivity. As the magnitude of $K_e$ is poorly constrained, we have varied this parameter in our simulations. While $K_\mathrm{e}$ might be expected to have meridional structure (likely increasing from pole to equator), we expect that only those simulations that have an overturning with a larger meridional extent, *e.g.* low values of $F_b$ and low latitude brine rejection ($\phi_b$), or high values of $\kappa$, would be sensitive to these variations.

We also include a representation of diabatic transport, which flows across density surfaces in the ocean interior and occurs due to mixing at scales smaller than the mesoscale. This vertical turbulent mixing is parameterized by a small-scale turbulent eddy diffusivity $\kappa$, which supports a vertical advection-diffusion balance in the ocean interior, $wb_z = (\kappa b_z)_z$. Note that subscripts $y$, $z$, and $t$ in this section are used to indicate partial derivatives. In the isopycnal model, the vertical velocity is approximated by

$$w(y) \approx \frac{\kappa}{\Delta z_n}, \tag{s5}$$

where $\Delta z_n$ is the thickness of the layer above the interface in question [4]. This approximation is valid if vertical variations in $\kappa$ are small relative to the buoyancy gradient ($\kappa_z b_z \ll \kappa b_{zz}$). The diabatic streamfunction is defined such that

$$\Psi_\mathrm{diabatic}(y) = \int_{S.\,pole}^{y} w(y')L(y')\,\mathrm{d}y'. \tag{s6}$$

The last term on the right-hand side of eq. s3 accounts for the buoyancy forcing at the ocean-ice interface. The buoyancy forcing arises from both differential heat uptake (changing the water temperature) and phase changes (changing salinity); we assume the latter to be the dominant cause of buoyancy differences on Enceladus. Phase changes (melting–refreezing of ice and aqueous exsolution–dissolution) must occur to compensate for processes that smooth out the meridional ice thickness gradients.

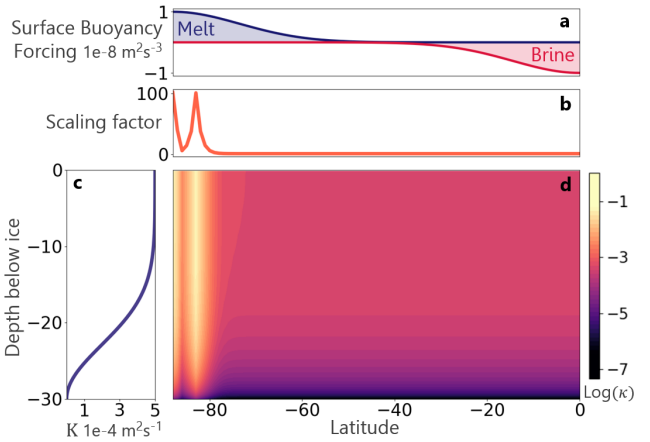


Fig. s2: Depiction of key model parameters for control run values. (a) The prescribed surface buoyancy forcing ($F_\mathrm{b}$) as a function of latitude for the southern hemisphere. The remaining panels show the components of the diapycnal diffusivity ($\kappa$). We include a scaling factor that varies with latitude (b), which is used in simulations that have enhanced polar mixing (plumes). $\kappa$ also has a vertical dependence (shown in c). The spatial distribution of $\kappa$ (logarithmic scale, e.g. $-1 = 10^{-1}$) is illustrated in the contour plot (d).

Over sufficiently long time scales, thick ice sheets deform plastically, leading to ice transport along the thickness gradient [5]. However, this flow is proportional to the gravitational force, which means it should be weak on a small moon such as Enceladus ($g = 0.113\ \mathrm{m\ s^{-2}}$), but could be significant on Europa ($g = 1.315\ \mathrm{m\ s^{-2}}$) and Titan ($g = 1.352\ \mathrm{m\ s^{-2}}$). An ice pump mechanism [6] could also be active, particularly for a thick shell in isostasy. The pump mechanism is fueled by the change in melt temperature as a function of pressure. Under the deeper regions of the ice shelf (at higher pressure) the melt point is lower, and the water at the interface is colder than that at shallower interfaces. If this cold water is displaced (by tides or other mechanisms), it will move

up to the shallower regions where it will serve as a heat sink and promote freezing. This process would tend to reduce thickness gradients in the ice shell at a rate proportional to the temperature gradient along the base of the ice shell. The rate is proportional to the interface depth variations, such that we would expect tens of meters of ice transport per Enceladus year, but the specific rate also depends on the ocean circulation itself. In order to sustain ice shell thickness gradients against such smoothing mechanisms, ice formation is required in thicker regions and melt in thinner regions. Thus, Enceladus' ice thickness pattern implies the existence of significant buoyancy forcing at the ocean-ice interface.

Water within density layers that intersect this mixed layer, or outcrop, is influenced by the buoyancy flux into the surface ocean that can give rise to water mass transformation. In the model, we prescribe a buoyancy flux $F_\mathrm{b}$ at the interface in each hemisphere of the form:

$$F_\mathrm{b}(y) = F_0\Big\{exp\Big[-\left(\frac{|y-\phi_m|}{\sigma}\right)^2\Big] - exp\Big[-\left(\frac{|y-\phi_b|}{\sigma}\right)^2\Big]\Big\}, \quad \text{(s7)}$$

where $F_0$ is the forcing magnitude (in m$^2$ s$^{-3}$). Regions of melt are centered at the poles ($|\phi_m| = 90^\circ =$ 396 km), and the forcing decays exponentially over a length scale of $\sigma = 90$ km. Regions of ice growth and brine rejection are centered at the equator ($\phi_b = 0^\circ =$ 0 km) for the control run, but are varied for other simulations. Transformation in the ocean surface boundary layer, and thus the meridional transport, is quantified by the relationship [7]:

$$\Psi_F = F_b(y)L(y)(b_y|_\mathrm{sfc})^{-1}, \quad \text{(s8)}$$

where the last term is the meridional buoyancy gradient within the ocean mixed layer.

With parameterizations for the terms in eq. s3 in hand, a solution for the ocean circulation can be determined by integrating in time to a steady state. In the mixed layer, where we have a buoyancy forcing and $b_z$ is by definition negligible, we can divide both sides of eq. s3 by the meridional buoyancy gradient at the interface ($b_y|_\mathrm{sfc}$), to get:

$$v_\mathrm{out.} = \frac{\partial y}{\partial t} = \frac{1}{h}\left(K_\mathrm{e}s - \frac{F_\mathrm{b}}{b_y|_\mathrm{sfc}}\right), \quad \text{(s9)}$$

which describes the time evolution of the outcrop location for each layer interface. Meanwhile, in the ocean interior, where there is no influence from the buoyancy forcing, we can divide by $b_z$ to arrive at:

$$w_\mathrm{int.} = \frac{\partial z}{\partial t} \approx \left(K_\mathrm{e}\frac{\partial s}{\partial y} + \frac{\kappa}{\Delta z}\right), \quad \text{(s10)}$$

where $w_\mathrm{int.}$ is the vertical velocity of the layer interface at a given location. Eq. s10 can also be derived directly from conservation of mass in the ocean interior.

The simulations presented in the paper were initialized with five layers. The buoyancy difference between each layer is $\Delta b = 4 \times 10^{-5}$ m s$^{-2}$. The layer interfaces were initially flat, shallow, and outcropped in the mid and high latitudes, in a region of prescribed sea ice melt. Various initial conditions were tested, including the use of deeper layers and outcrops in regions of ice formation. These simulations achieved the same steady state solutions, suggesting that solutions are not sensitive to initial conditions.

The ocean interior is modeled on a semi-adaptive grid in which each layer interface has a fixed number of meridional grid points. Thus, the vertical resolution is determined by the number of buoyancy layers. The meridional resolution is adjustable and set to 2° for this work. The ocean-ice interface depth varies in accordance with the prescribed ice structure described above. For the simulations we present in this study, we assume symmetry about the equator and run a single hemisphere. We also prescribe a sinusoidal structure to the interface (fig. 2a), such that the difference in depth between equator and pole is $\Delta_\mathrm{ice}$. Simulations with different structures and various values of $\Delta_\mathrm{ice}$ were tested, but have not been included because effects on the ocean structure and flow are small. The outcrop locations are allowed to vary freely, independent of the interior grid. The model accounts for changes in the zonal extent of latitude circles between the equator and pole to ensure conservation of volume. The model also accounts for changes in circumference with depth, though this feature is not significant for the range of parameters explored in this work.

Through the assumption of zonal symmetry, this model does not explicitly include zonal flows. We would expect a zonal flow to be present on Enceladus and perhaps, as is the case in Earth's Southern Ocean, it could even be stronger than the meridional circulation. However, for the purposes of understand-

ing heat and nutrient transport, the meridional flow is most relevant and is thus the focus of this work. A strong zonal flow, or even zonal jets [8] may coexist with our modeled meridional circulation in the ocean interior. If the zonal flow at the ocean-ice boundary were sufficiently strong, it could produce a frictional stress and a meridional Ekman transport near the boundary [7]. This transport has not been not included in the model but could be easily incorporated in our residual circulation framework, as has already been done in Southern Ocean models that include a wind-driven Ekman transport [4].

We summarize the processes described above as two key balances: (i) the flow in the ocean interior either towards or away from the ocean-ice interface must balance the water mass transformation in the mixed layer. Until this balance is met, any net convergence in the mixed layer will induce density layer outcrop displacement. (ii) Any net volume transport, through vertical mixing, into a density layer in the ocean interior must be transported along the layer and eventually flow into the mixed layer. If a divergence in the adiabatic transport is not balanced locally by a convergence in the diabatic transport, the volume flux convergence within a layer induces a change in layer depth. Once the layers reach equilibrium, the net flow into and out of each layer must exactly cancel by mass conservation. Though we do not track the flow below the bottom layer, the vertical fluxes are balanced such that mass is conserved everywhere. Note that at steady state, the diabatic transport across a given interface (shown in fig. 3) is balanced by the total adiabatic lateral transport above that level, such that $\Psi_{\text{diabatic}} = -\Psi_{\text{adiabatic}} = K_{\text{e}}(s - s_{\text{ice}})2\pi\cos\phi$. Finally, the equilibrium solution requires that (eq. s9) and (eq. s10) are identically zero.

Our control run, shown in fig. 2 and 3, utilizes the parameters shown in fig. 1 and listed in Table s1. The latter also itemizes the full range of parameters explored in fig. 4, plus the range of meridional ice thickness gradients ($\Delta_{\text{ice}}$) that were studied. Note that we are only modeling a few discreet layers, which limits our resolution of the circulation patterns. Our parameters were selected to facilitate comparison over a wide range of simulations, but future work that incorporates the deeper-ocean circulation, and especially dynamics at the ocean-core interface, would likely require considerably more layers.

| **Model Parameter** | **Control Value** | **Min** | **Max** |
|---|---|---|---|
| $\Delta b$ | $4 \times 10^{-5}$ m s$^{-2}$ | - | - |
| $K_{\text{e}}$ | $10^{3}$ m$^{2}$ s$^{-1}$ | 200 m$^{2}$ s$^{-1}$ | 5000 m$^{2}$ s$^{-1}$ |
| $\kappa$ | $5 \times 10^{-4}$ m$^{2}$ s$^{-1}$ | $10^{-4}$ m$^{2}$ s$^{-1}$ | $10^{-2}$ m$^{2}$ s$^{-1}$ |
| $\Delta$ice | 10 km | 1 km | 20 km |
| $\phi_b$ | $0^{\circ}$ | $0^{\circ}$ | $60^{\circ}$ |
| $F_0$ | $10^{-8}$ m$^{2}$ s$^{-3}$ | $10^{-10}$ m$^{2}$ s$^{-3}$ | $10^{-7}$ m$^{2}$ s$^{-3}$ |

Table s1: Simulation parameters for control run and the range of values tested for parameters that were explored.

## S.2 Ocean Temperature and Salinity

Our control model parameters (Table s1) were initially selected based on Earth-like values, although the value of $\Delta b$ was intentionally chosen to be small. Given that Enceladus' ocean is nearly an order of magnitude deeper than Earth's, our parameters were optimized for a weak stratification. However, we find that the isopycnals concentrate in the upper portion of the ocean in the control simulation, producing stronger stratification near the interface and weaker stratification in the deep ocean. We do not account for bottom boundary processes that could affect the deeper ocean density structure.

The buoyancy gradients in the upper ocean could occur due to variations in temperature, salinity, or a combination of both. Our model does not distinguish between these scenarios. However, for the predicted pressure and temperature range in Enceladus' ocean (fig. s3, left), the equations of state predict that the density variations are almost entirely controlled by salinity.

Using the linearized equation of state, a thermal expansion coefficient $\alpha = 5.788 \times 10^{-5}$ K$^{-1}$ and a saline contraction coefficient $\beta = 7.662 \times 10^{-4}$ kg g$^{-1}$ (obtained using TEOS-10 for 20 MPa), we can verify the changes required to produce a buoyancy difference of $\Delta b = 4 \times 10^{-5}$ m s$^{-2}$ (the difference between two sequential layers). These coefficients were obtained using a base temperature of 274 K, a degree higher than estimated in the literature [9], to remove negative thermal expansivity arising from the lower assumed salinity of 12 ppt consistent with *Cassini* measurements [10]. These effects are probably relevant near the ice shell [11], but are beyond the scope of this work. Under these conditions, if the ocean had constant salinity, a 6 K temperature difference would be required between layers (30 K overall). This is more than three times the temperature difference required for Earth-like conditions (1.7K). Whereas, for an isothermal ocean, a 0.46 g kg$^{-1}$ salinity change between layers could account for the difference in buoyancy (fig. s3, right).

Assuming that temperature variations in the bulk of the ocean are limited to less than 4 K [9], the buoyancy differences modeled in this work and the ensuing circulation can be attributed almost entirely to salinity differences. The total variation in salinity between our lowest density layer and our highest density layer is estimated to be roughly 2 g kg$^{-1}$. Further constraints could be obtained in future work through the use of additional model layers.

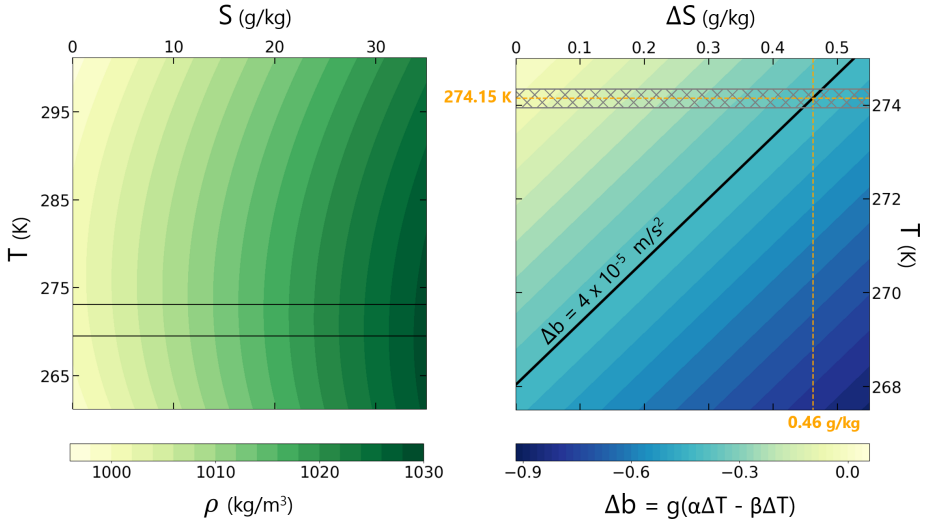


Fig. s3: (Left) Predicted density for various temperatures and salinities at 20 MPa. The black lines highlight the temperature range relevant for Enceladus [9]. (Right) Equivalent change in temperature and salinity to produce the buoyancy difference ($\Delta_b$) between layers in the model, calculated at 20 MPa, with a mean temperature of 274.15 K. The black line highlights the model's $\Delta b$. For comparison, the grey hatching shows the expected variations in ocean temperature if the composition is kept constant (obtained using TEOS-10).

## Supplemental References


[1] Sjoerd Groeskamp et al. "The Water Mass Transformation Framework for Ocean Physics and Biogeochemistry". *Annual Review of Marine Science* (2019), pp. 271–305. DOI: 10.1146/annurev-marine-010318-095421.

[2] P. R. Gent and J. C. McWilliams. "Isopycnal mixing in ocean circulation models". *J. Phys. Oceanogr.* (1990), pp. 150–155.

[3] G. K. Vallis. *Atmospheric and Oceanic Fluid Dynamics*. Cambridge, U.K.: Cambridge University Press, 2006, p. 745.

[4] Andrew F Thompson, Sophia K Hines, and Jess F Adkins. "A Southern Ocean Mechanism for the Interhemispheric Coupling and Phasing of the Bipolar Seesaw". *Journal of Climate* (Apr. 2019), pp. 4347–4365. DOI: 10.1175/JCLI-D-18-0621.1.

[5] Jason C. Goodman. "Glacial flow of floating marine ice in "Snowball Earth"". *Journal of Geophysical Research* 108 (2003), pp. 1–12. DOI: 10.1029/2002jc001471.

[6] E. L. Lewis and R. G. Perkin. "Ice pumps and their rates". *Journal of Geophysical Research: Oceans* (1986), pp. 11756–11762. DOI: 10.1029/JC091iC10p11756.

[7] John Marshall and Timour Radko. "Residual-Mean Solutions for the Antarctic Circumpolar Current and Its Associated Overturning Circulation". *Journal of Physical Oceanography* 33.11 (2003), pp. 2341–2354. DOI: 10.1175/1520-0485(2003)033<2341:RSFTAC>2.0.CO;2.

[8] K. M. Soderlund et al. "Ocean-driven heating of Europa's icy shell at low latitudes". *Nature Geoscience* (2014), pp. 16–19. DOI: 10.1038/ngeo2021.

[9] Steven D. Vance et al. "Geophysical Investigations of Habitability in Ice-Covered Ocean Worlds". *Journal of Geophysical Research: Planets* 123.1 (2018), pp. 180–205. DOI: 10.1002/2017JE005341.

[10] CR Glein, F Postberg, and SD Vance. "The Geochemistry of Enceladus: Composition and Controls". University of Arizona Press, 2019, pp. 39–56.

[11] H. J. Melosh et al. "The temperature of Europa's subsurface water ocean". *Icarus* (2004), pp. 498–502.